HDPE and TiO_2 with and without γ-MPS treatment were introduced into the heated chamber simultaneously. The rotor speed was fixed at 25 rpm. The total mixing process lasted about 30 min.

2.2. Preparation of TiO_2/HDPE composites

The manufacturing process of TiO_2/HDPE with γ-MPS involved kneading and compression molding. The filler content was set at 40 vol% because the composite with this composition shows both bioactivity and mechanical properties analogous to those of human cortical bone [17]. This composite was denoted as TiO_2/HDPE-40. HDPE was dried at 80 °C for 8 h and then kneaded at 210 °C in a batch kneader PBV 0.3 (Irie Shokai, Ltd., Tokyo, Japan). TiO_2 particles were added slowly into the melted HDPE with kneading at 210 °C in air. After adding TiO_2, TiO_2/HDPE compound was kneaded at 25 rpm for 30 min.

The obtained compounds were molded at 230 °C for 1 h and then hot-pressed in air at pressures between 2.5 and 5.8 MPa. TiO_2/HDPE composite without γ-MPS was also produced via the same route for comparison purposes.

2.3. Characterization of TiO_2/HDPE composites

2.3.1. Fourier transform infrared spectroscopy

The spectra of the TiO_2/HDPE-40 composite with and without γ-MPS hot-pressed at 2.5 MPa were analyzed with a FT-IR spectrophotometer FT/IR-550 (JASCO Co., Osaka, Japan). The hot-pressed composite surface was ground and dispersed in a matrix of KBr, followed by compression to consolidate the formation of the pellet. FT-IR spectra were obtained by the KBr pellet method in the wave-number range from 400 to 4000 cm^{-1} with a resolution of 4 cm^{-1}.

2.3.2. SEM observation

The fracture surfaces of TiO_2/HDPE-40 composites with and without γ-MPS hot-pressed at 2.5 MPa were examined using the field emission scanning electron microscope (FE-SEM) JSM-633OF (JEOL DATUM Co. Ltd., Nagoya, Japan) after coating them with a thin Au film.

2.3.3. Mechanical test

Three-point bend testing was performed using five samples of each type of composite. The specimens were cut to the desired shape and then polished, using 400 grit silicon carbide paper, to a size of 40 mm × 10 mm × 4 mm. A testing machine, Model 5582 (Instron Co. Ltd., LA, USA), was used to apply a load over a 30 mm span. Measurements were performed with a cross-head speed of 1.0 mm/min at room temperature, according to JIS K 7171. Bending yield strength was calculated as [14,23]

$$\text{Bending yield strength,}\quad \sigma_f = \left(\frac{3p_fL}{2bd^2}\right)\left(\frac{n+2}{3}\right) \tag{1}$$

p_f is the load at fracture (N), L is the sample length (mm), b is the sample width (mm), d is the sample height (mm), and n is a strain-hardening exponent ($0 < n < 1$). The strain-hardening exponent n was estimated as the slope of log–log plot of p versus δ in the nonlinear region of the load–displacement curve. δ is the deflection of the specimen at mid-span (mm).

The Young's modulus was estimated from the slope of the initial linear elastic region of the load–displacement curve.

2.3.4. Density

The density of TiO_2/HDPE-40 composite was measured by the Archimedes method using a pycnometer and a glass bottle of known volume with a capillary tube at the top as a container. The liquid medium was distilled water for all materials.

3. Results

3.1. Torque of composites

It is known that melt viscosity can be related to the torque measured by the equipment during blending [24]. Fig. 1 shows a plot of torque versus time for TiO_2/HDPE-40 with (a) and without (b) γ-MPS. The introduction of cold HDPE

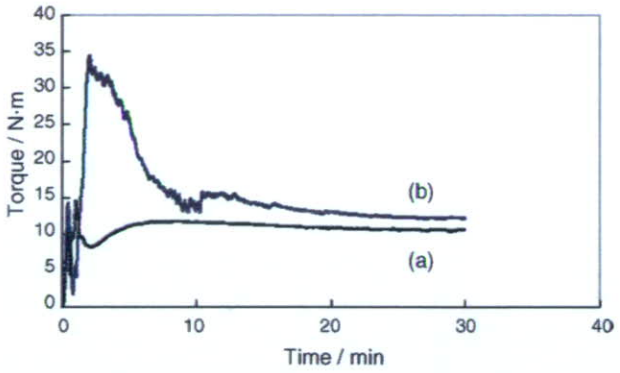

Fig. 1. Plot of torque vs. time for TiO_2/HDPE-40 composites with (a) and without (b) γ-MPS at 200 °C.

and TiO_2 into the preheated mixer chamber initially led to an increase of torque, followed by a decrease of torque during the fusion of HDPE (Fig. 1(a) and (b)). The torque of TiO_2/HDPE-40 without γ-MPS became approximately constant after about 10 min (Fig. 1(b)). On the other hand, the system containing γ-MPS showed lower and variable torque during experiments (Fig. 1(a)). The addition of γ-MPS decreased the torque during the first 2–3 min due to the plasticizing effect of the silanized TiO_2. This torque slowly increased with processing, probably due to chain branching reactions induced by heat and mechanical forces. The torque of TiO_2/HDPE-40 composite with γ-MPS was lower than that of composite without γ-MPS after blending for 30 min. Therefore, a silane-coupling agent such as γ-MPS produced a lower viscosity TiO_2/HDPE-40 composite, as can be seen from curve (a).

3.2. FT-IR spectra of composites

Fig. 2 shows the characteristic spectra of TiO_2/HDPE-40 with (a) and without (b) γ-MPS. It shows the bands involved in the interfacial interaction between the TiO_2 particles and the HDPE matrix in the presence or absence of γ-MPS. Upon comparing the composite spectra, differences in the shape and position of the bands can be observed.

The most significant bands of the TiO_2 particles studied and the assignment for each one are a broad adsorption band between 500 and 1000 cm^{-1} attributed to Ti–O–Ti linkages in TiO_2 nanoparticles [25,26]. On the other hand, in the HDPE spectrum, it is necessary to highlight the band at 1474 cm^{-1} ($-CH_2$) [27] and the characteristic band at 1386 cm^{-1} (wagging $-CH_2$) [27]. In Fig. 2, one special band at 1720 cm^{-1} and a slightly different shape at 900–1300 cm^{-1}, corresponding to neither TiO_2 particles nor HDPE, are observed only for the composite with γ-MPS (a). Also, the bands at 3085 cm^{-1} and 3025 cm^{-1} are observed for the composite without γ-MPS (b).

Fig. 3 shows the FT-IR spectra in the 1300–2000 cm^{-1} region of the TiO_2/HDPE-40 composite hot-pressed at 2.5 MPa with (a) and without (b) γ-MPS. As shown in Fig. 3(a), the spectral band at 1720 cm^{-1} was attributed to the carboxyl group of γ-MPS. This result indicates the applicability of silane coupling on the surface of TiO_2 particles. The spectral band at 1654 cm^{-1} corresponds to water absorption due to the hydrophilic character of the TiO_2 particles (Fig. 3(a) and (b)).

Fig. 4 shows the FT-IR spectra in the 900–1300 cm^{-1} region of the TiO_2/HDPE-40 composite hot-pressed at 2.5 MPa with (a) and without (b) γ-MPS. The spectral band at 1162 cm^{-1} was attributed to an ether bond (C–O–C). Also, two broad bands appear at 1106 and 1035 cm^{-1}, which are assigned to Si–O stretching vibration, indicating the generation of a Si–O–Si network [28]. The absorption peak at about 940 cm^{-1} corresponds to Si–O–Ti stretching vibration [29,30].

Fig. 5 shows the FT-IR spectra in the 2700–3300 cm^{-1} region of the TiO_2/HDPE-40 composite hot-pressed at 2.5 MPa with (a) and without (b) γ-MPS. The 2946 cm^{-1} band is assigned to the symmetric stretching of CH_2 in HDPE for composites containing 40 vol% of TiO_2 (Fig. 5(a) and (b)). The bands at 3085 and 3025 cm^{-1}, corresponding to the bending of the vinyl group in HDPE, are reduced in the case of TiO_2/HDPE-40 with γ-MPS (Fig. 5(a)).

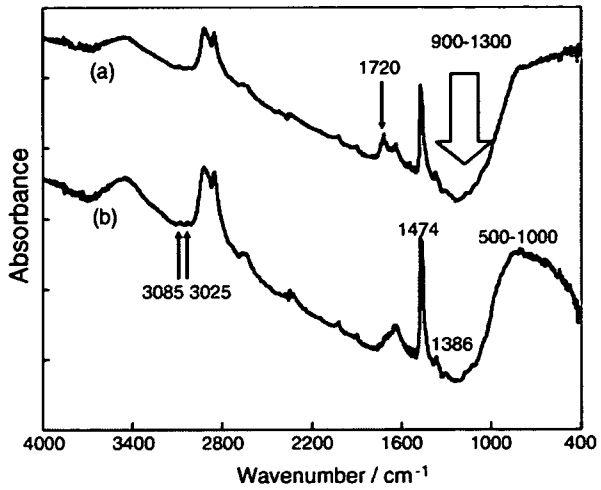

Fig. 2. FT-IR spectra of TiO_2/HDPE-40 composites with (a) and without (b) γ-MPS.

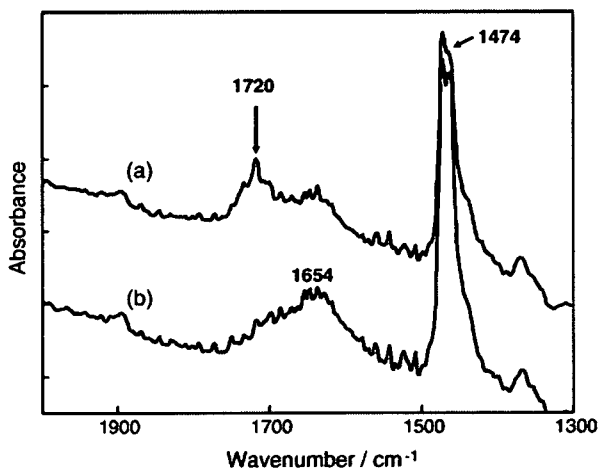

Fig. 3. FT-IR spectra in the 1300–2000 cm^{-1} region for TiO_2/HDPE-40 composites with (a) and without (b) γ-MPS.

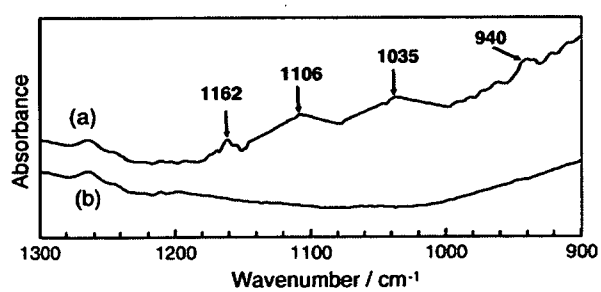

Fig. 4. FT-IR spectra in the 900–1300 cm^{-1} region for TiO_2/HDPE-40 composites with (a) and without (b) γ-MPS.

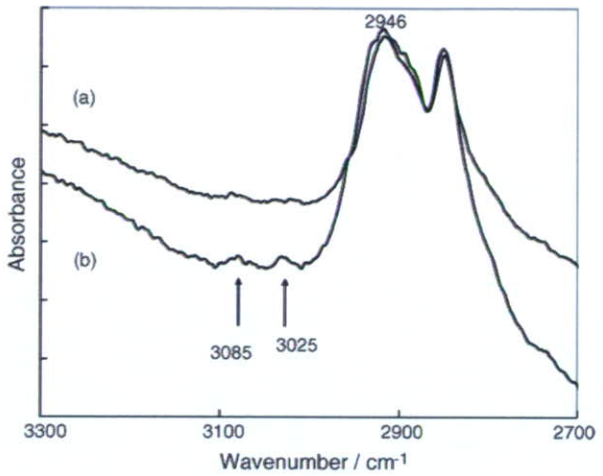

Fig. 5. FT-IR spectra in the 2700–3300 cm^{-1} region for TiO_2/HDPE-40 composites with (a) and without (b) γ-MPS.

3.3. SEM characterization of composites

Fig. 6 shows FE-SEM images of the fracture surfaces of TiO_2/HDPE-40 with (a) and without (b) γ-MPS after the bending test. This figure shows the effect of a tensile load on local deformation of HDPE around the TiO_2 particles in each of the composites. As the FE-SEM image in Fig. 6(a) shows, HDPE covered the surface of individual TiO_2 particles, indicating that a chemical bond existed between TiO_2 and HDPE. However, for TiO_2/HDPE without γ-MPS (Fig. 6(b)), no residual HDPE was found on the TiO_2 particles.

3.4. Mechanical properties of composites

The bending yield strength and Young's modulus of TiO_2/HDPE-40 with (a) and without (b) γ-MPS as a function of hot-pressing (HP) pressure are shown in Figs. 7 and 8, respectively. In the case of TiO_2/HDPE-40 without γ-MPS, the bending yield strength and Young's modulus were independent of HP pressure (Figs. 7(b) and 8(b)). On the other hand, the bending yield strength and Young's modulus of TiO_2/HDPE-40 with γ-MPS increased with increasing HP pressure up to 5 MPa and decreased at pressures higher than 5.7 MPa. The bending yield strength and Young's modulus, respectively, were 49 MPa and 7.5 GPa for the HP pressure of 2.5 MPa, 58 MPa and 8 GPa for the HP pressure of 4.5 MPa, 65 MPa and 10 GPa for the HP pressure of 5 MPa, and 61 MPa and 7 GPa for the HP pressure of 5.7 MPa.

The representative load–displacement curves were obtained for HDPE, and TiO_2/HDPE-40 without (Fig. 9) and with γ-MPS (Fig. 10) by three-point bend testing. Pure HDPE did not fracture within the limits of the three-point

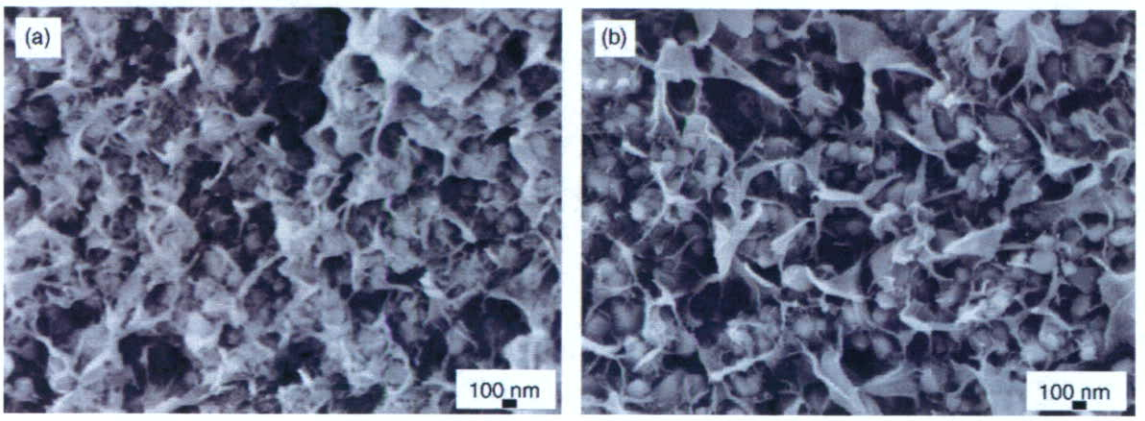

Fig. 6. Scanning electron micrographs of fracture surfaces of TiO_2/HDPE-40 composites with (a) and without (b) γ-MPS.

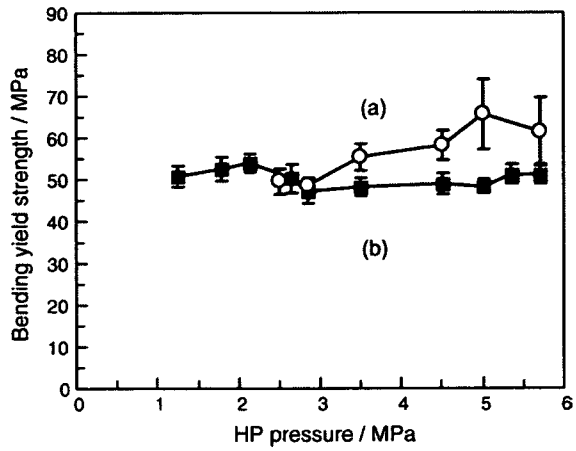

Fig. 7. Bending yield strength of TiO_2/HDPE-40 composites with (a) and without (b) γ-MPS as a function of hot-pressing pressure.

bending apparatus. This behavior indicated the mechanical properties of low bending yield strength and Young's modulus, and large strain to failure. For TiO_2/HDPE-40 without γ-MPS (Fig. 9), it can be noted that all the curves exhibit nearly linear behavior independent of HP pressure. All the composites break in a brittle manner when the load reaches a maximum. However, for TiO_2/HDPE-40 with γ-MPS (Fig. 10), all the curves exhibit the non-linear behavior of a ductile matrix. Once the load reaches its maximum value there are clearly significant differences in the way these

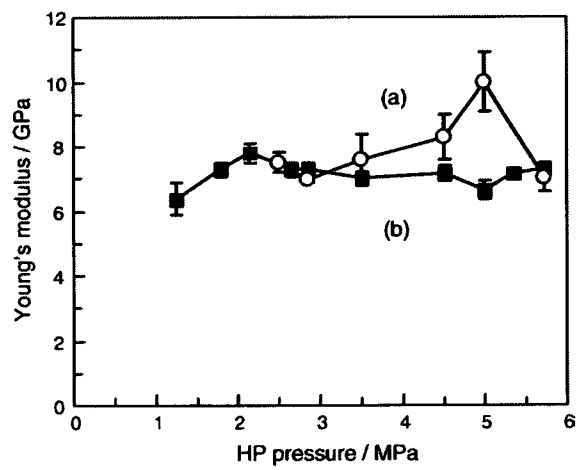

Fig. 8. Young's modulus of TiO_2/HDPE-40 composites with (a) and without (b) γ-MPS as a function of hot-pressing pressure.

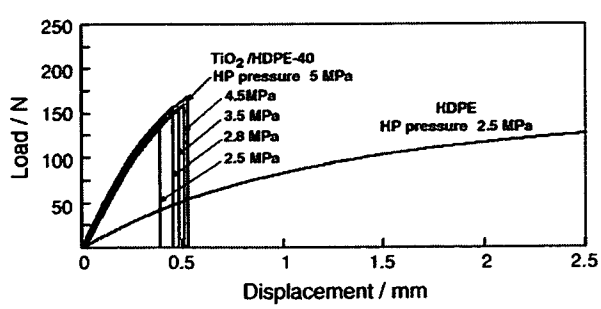

Fig. 9. Load–displacement curve of TiO_2/HDPE-40 composite without γ-MPS hot-pressed at various pressures and that of pure HDPE.

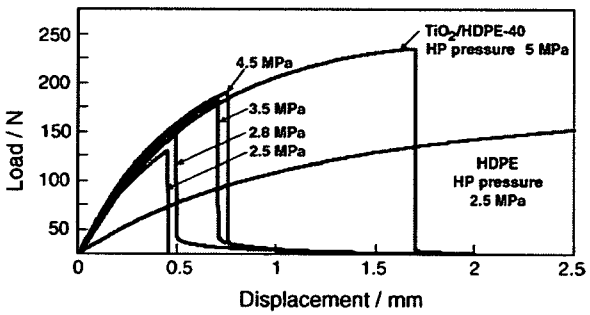

Fig. 10. Load–displacement curve of TiO_2/HDPE-40 composite with γ-MPS hot-pressed at various pressures and that of pure HDPE.

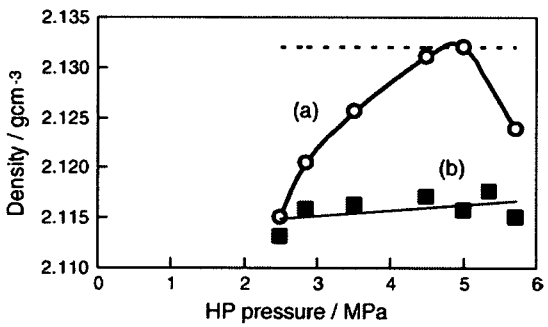

Fig. 11. Density of TiO_2/HDPE-40 composite with (a) and without (b) γ-MPS as a function of pressure applied during shaping (dotted line represents the theoretical density value of 2.132 g/cm^3).

curves decrease. The load–displacement curve depicts a weakly bonded interphase after the interphase fails (HP pressure 2.5 MPa). The TiO_2 particles were separated from the matrix in a controlled manner and friction was measured until all TiO_2 particles were completely removed (HP pressure: 2.8, 3.5 and 4.5 MPa). Fig. 10 shows that the load–displacement curve for silane-treated composite (HP pressure 5 MPa) indicates a very strongly bonded interphase; the interface failed immediately after complete TiO_2 particle separation.

3.5. Density of composites

Fig. 11 shows the densities of the TiO_2/HDPE-40 composites with (a) and without (b) γ-MPS as a function of HP pressure. Compared with the theoretical density (denoted by the dotted line), which was calculated using the rule of mixture, the density of TiO_2/HDPE with γ-MPS (a) increased with HP pressure up to almost identical value to the theoretical one (2.132 g/cm^3) at 5 MPa. However, as the hot-pressing pressure was increased to 5.7 MPa, the discrepancy between the measured and theoretical densities increased. In contrast, the density of TiO_2/HDPE without γ-MPS (b) was independent of HP pressure.

4. Discussion

The mechanical strength of TiO_2/HDPE-40 was enhanced by both the silanation of TiO_2 and the increase of the HP pressure applied to shape the composite.

The TiO_2/HDPE composite without γ-MPS presents very weak physicomechanical adhesion, as shown in Fig. 6(b). For the fracture surface of the TiO_2/HDPE composite, no residual HDPE was found on the TiO_2 particles, indicating that no chemical bond existed between the matrix and filler. Therefore, the voids form at the particle–matrix interface, first in the direction of the applied stress. This void then grows and merges as shear stresses deform the rest of the matrix, leading to the eventual failure of the composites. This result was consistent with the model proposed by Juhasz et al. for an apatite–wollastonite-reinforced HDPE composite with no interfacial bonding [15]. Hence stress transfer

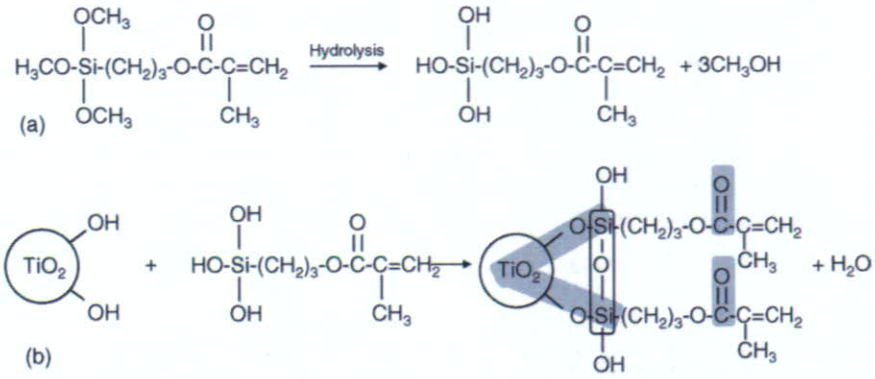

Fig. 12. Scheme of hydrolyzation of γ-MPS and absorption of hydrolyzed alkoxysilanol on TiO_2.

does not take place between TiO_2 and HDPE. On the other hand, for the silanated TiO_2/HDPE composite, as shown in Fig. 6(a), the silane-coupling agent facilitates direct contact between the TiO_2 particles and the HDPE matrix to a higher degree than the contact in the untreated composite. It can also be observed that the composites broke due to shear yield and tearing. The differences between the failure surfaces of differently treated composites are attributed to the different chemical natures of the coupling agent and the different adhesion mechanisms.

In the silanated TiO_2/HDPE composite, as shown in Fig. 4(a), the bands of 1035 and 1106 cm^{-1} are mainly attributed to Si–O–Si vibration. The silane-coupling agent undergoes chemical changes during hydrolysis and drying. During hydrolysis of the silane, the $SiOCH_3$ group will transform into SiOH, as shown in Fig. 12(a). Then, the hydrolyzed alkoxysilanol can be absorbed into the surface and condenses with the hydroxyl group of TiO_2 components, as shown in Fig. 12(b). The hydrolyzed alkoxy silanes can undergo condensation and bond formation. Besides these reactions of the silanol and the hydroxyl groups of the TiO_2 surface, the formation of the siloxane structure can also occur, which gives rise to the band at 940 cm^{-1} attributed to Si–O–Ti (Fig. 4(a)). This reveals the formation of a covalent bond between the silane-coupling agent and the TiO_2 particles.

Fig. 5 shows the evolution of the reduced absorbance corresponding to the bending of the vinyl group (–CH=CH_2, 3025 and 3085 cm^{-1}). This seems to correspond to the reactivity between the double bond of HDPE and those of the coupling agent on TiO_2 particles, as shown in Fig. 13. Therefore, HDPE covered the surface of individual TiO_2 particles, as shown in Fig. 6(a).

Homogeneous dispersion of nanoparticles in a polymeric matrix is very difficult due to the strong tendency of nanoparticles to agglomerate. Consequently, the so-called nanoparticle-filled polymers sometimes contain a number of loosened clusters of particles. It can be seen that in the silane-treated composite, HDPE penetrated into the cavity between TiO_2 particles because of its low viscosity in the molten state (Fig. 1). This seems to indicate that wetting of the TiO_2 particles plays a key role in TiO_2 and HDPE matrix adhesion because it increases the degree of mechanical

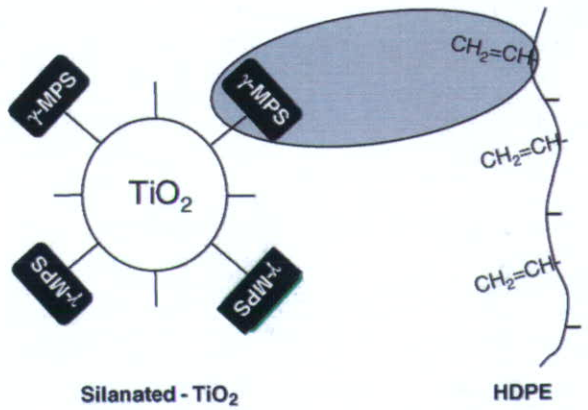

Fig. 13. Adhesion mechanism for silane-treated TiO_2 and HDPE.

interlocking. This means that proper TiO_2 wetting by γ-MPS and an increased hot-pressing pressure could explain the increment of the density of the composites (Fig. 11(a)).

These studies revealed that the final mechanical strengths are determined by two competing factors: one is the increase in compatibility between TiO_2 and HDPE due to the presence of the silane-coupling agent, and the other is the increase in the density of the composite. Also, with high strain (pressure applied during shaping is higher than 5 MPa), the properties of the composite seemed to be deteriorated because high strain leads to the formation of cracks and fractures at interphase boundaries. Therefore, the mechanical strengths of TiO_2/HDPE composite decreased due to the decrease of density.

5. Conclusions

The bending yield strength and Young's modulus increased with the increase of the pressure applied during shaping only for the silane-treated TiO_2/HDPE composite (maximum bending yield strength = 65 MPa, Young's modulus = 10 GPa). γ-MPS has a higher capacity to form the covalent bond, that is, an ether bridge (1162 cm^{-1}). The vinyl groups of HDPE reacted with the double bonds within γ-MPS. Increasing the pressure applied during shaping resulted in an increase in the density of silane-treated TiO_2/HDPE composite. These chemical interactions between TiO_2 and HDPE and the disappearance of voids and cracks resulted in better mechanical performance of silane-treated TiO_2/HDPE composite.

Acknowledgement

This work is supported in part by the National Research and Development Programs for Medical and Welfare Apparatus entrusted by the New Energy and Industrial Technology Development Organization (NEDO) to the Japan Fine Ceramics Center.

References

[1] L.L. Hench, R.J. Splinter, W.C. Allen, T.K. Greenlee Jr., J. Biomed. Mater. Res. 2 (1971) 117–141.
[2] M. Jarcho, J.L. Kay, R.H. Gumaer, H.P. Drobeck, J. Bioeng. 1 (1977) 79–92.
[3] T. Kokubo, M. Shigematsu, Y. Nagashima, M. Tashiro, T. Nakamura, T. Yamamuro, S. Higashi, Bull. Inst. Chem. Res. Kyoto Univ. 60 (1982) 260–268.
[4] T. Kokubo, S. Ito, M. Shigematsu, S. Sakka, T. Yamamuro, J. Mat. Sci. 20 (1985) 2001–2004.
[5] T. Kokubo, S. Ito, M. Shigematsu, S. Sakka, T. Yamamuro, J. Mat. Sci. 22 (1987) 4067–4070.
[6] K. Ono, T. Yamamuro, T. Nakamura, T. Kokubo, Biomaterials 11 (1990) 265–271.
[7] T. Yamamuro, J. Shikata, H. Okumura, T. Kitsugi, Y. Kakutani, T. Matsui, T. Kokubo, J. Bone Joint Surg. 72-B (1990) 889–893.
[8] H.M. Kim, F. Miyaji, T. Kokubo, T. Nakamura, J. Biomed. Mater. Res. 32 (1996) 409–417.
[9] M. Uchida, H.M. Kim, T. Kokubo, S. Fujibayashi, T. Nakamura, J. Biomed. Mater. Res. 63 (5) (2002) 522–530.
[10] W. Bonfield, M.D. Grynpas, A.E. Tully, J. Bowman, J. Abram, Biomaterials 2 (1981) 185–186.
[11] M. Wang, R. Joseph, W. Bonfield, Biomaterials 19 (1998) 2357–2366.
[12] M. Wang, W. Bonfield, Biomaterials 22 (2001) 1311–1320.
[13] M. Wang, Biomaterials 24 (2003) 2133–2151.
[14] J.A. Juhasz, S.M. Best, W. Bonfield, M. Kawashita, N. Miyata, T. Kokubo, T. Nakamura, J. Mater. Sci.—Mater. Med. 14 (2003) 489–495.
[15] J.A. Juhasz, S.M. Best, R. Brooks, M. Kawashita, N. Miyata, T. Kokubo, T. Nakamura, W. Bonfield, Biomaterials 25 (2004) 949–955.
[16] H. Takadama, M. Hashimoto, Y. Takigawa, M. Mizuno, Y. Yasutomi, T. Kokubo, Key Eng. Mater. 254–256 (2004) 569–572.
[17] M. Hashimoto, H. Takadama, M. Mizuno, T. Kokubo, J. Mater. Sci.—Mater. Med., Submitted for publication.
[18] S. Jose, A.S. Aprem, B. Trancis, M.C. Chandy, P. Werner, V. Alstaedt, S. Thomas, Eu. Polym. J. 40 (2004) 2105–2115.
[19] B. Pukanszky, E. Fekete, F. Tudos, Chemie Macromolecular Symposia 28 (1989) 165–186.
[20] J. Jancar, J. Kucera, Polym. Eng. Sci. 30 (12) (1990) 707–713.
[21] J. Jancar, J. Kucera, Polym. Eng. Sci. 30 (12) (1990) 714–720.
[22] E.P. Plueddemann, Silane Coupling Agents, 3rd ed., Plenum Press, New York, 1991.
[23] N.E. Dowling (Ed.), Engineering Materials For Deformation, Fracture and Fatigue, Prentice-Hall Inc., Englewood Cliffs, NJ, 1993, pp. 570–617 (Chapter 13).
[24] F.W. Fabris, F.C. Stedile, R.S. Mauler, S.M.B. Nachtigall, Eu. Polym. J. 40 (2004) 1119–1126.
[25] C. Xie, Z. Xu, Q. Yang, B. Xue, Y. Du, J. Zhang, Mater. Sci. Eng., B 112 (2004) 34–41.
[26] T. Bezrodna, G. Puchkovska, V. Shymanovska, J. Baran, H. Ratajczak, J. Mol. Struct., in press.
[27] X. Colom, F. Carrasco, P. Pages, J. Canavate, Compos. Sci. Technol. 63 (2003) 161–169.
[28] B.B. Johnsen, K. Olafsen, A. Stori, Int. J. Adhes. Adhes. 23 (2003) 155–163.
[29] B. Bai, J. Zhao, X. Feng, Mater. Lett. 57 (2003) 3914–3918.
[30] G. Gu, Z. Zhang, H. Dang, Appl. Surf. Sci. 221 (2004) 129–135.

Phospholipid polymer surfaces reduce bacteria and leukocyte adhesion under dynamic flow conditions

Jasmine D. Patel,[1] Yasuhiko Iwasaki,[2] Kazuhiko Ishihara,[3] James M. Anderson[1,4]
[1]*Department of Biomedical Engineering, Case Western Reserve University, Cleveland, Ohio 44106*
[2]*Institute of Biomaterials and Bioengineering, Tokyo Medical and Dental University, 2-3-10 Kanda-urugadai, Chiyoda-ku, Tokyo 101-0062, Japan*
[3]*Department of Materials Engineering, School of Engineering, The University of Tokyo, 7-3-1 Hongo, Bukyo-ku, Tokyo 113-8656, Japan*
[4]*The Institute of Pathology, Case Western Reserve University, 2085 Adelbert Road, Room 306, Cleveland, Ohio 44106*

Received 20 December 2004; accepted 3 January 2005
Published online 30 March 2005 in Wiley InterScience (www.interscience.wiley.com). DOI: 10.1002/jbm.a.30302

Abstract: Persistence of infection can occur when the host immune response is compromised because of the presence of a foreign implant. Surface modification of biomaterials with phospholipid polymers may enhance biocompatibility and reduce incidence of infection by impeding bacterial and leukocyte adhesion. A rotating disk model, which generates shear stress from 0 to 18 dynes/cm^2, was used to characterize adhesion of neutrophils, monocytes, and bacteria in phosphate-buffered saline (PBS) or 25% human serum on polyethylene terephthalate surfaces coated with a phospholipid polymer, poly[ω-methacryloyloxyalkyl phosphorylcholine (MAPC)-*co*-*n*-butyl methacrylate (BMA)]. The material designated PMB30 contains a methylene chain length, $(CH_2)_n$, of $n = 2$, whereas PMHB30 contains a chain length of $n = 6$. In PBS, bacterial adhesion was shear stress dependent with the lowest bacterial density observed on PMB30. However, the presence of serum proteins eliminated shear stress and surface chemistry effects in addition to bacterial adhesion reduced to <10% of adhesion in PBS. Trends for leukocyte adhesion in serum demonstrated shear dependence with PMB30 exhibiting the lowest cell density throughout the range of shear stresses. In conclusion, modification of the polyethylene terephthalate surfaces with phospholipid polymers resulted in reduced bacterial and leukocyte adhesion. Furthermore, shortening the methylene chain length of the MAPC copolymer most effectively reduced adhesion. © 2005 Wiley Periodicals, Inc. J Biomed Mater Res 73A: 359–366, 2005

Key words: infection; shear stress; phospholipid polymers; *Staphylococcus epidermidis*; leukocytes

INTRODUCTION

Infection is a serious complication associated with implanted medical devices. Coagulase-negative staphylococci, in particular, *Staphylococcus epidermidis*, are among the most common bacteria isolated from infected implants. Persistence of infection can occur when the host immune response is compromised because of the presence of a foreign implant and the high resistance of biomaterial-adherent bacteria to antibiotic therapy.[1–4]

Infection develops from initial bacterial adhesion on the surface of the implant, followed by bacterial aggregation, proliferation, and exopolysaccharide slime production.[5] Biofilm formation, more specifically the barrier of slime, contributes to the pathogenicity of indwelling device infection by impeding access of leukocytes and antibiotics to the adherent bacteria.[2,6] Therefore, it is critical to inhibit initial bacterial adhesion to biomaterials to prevent the development of chronic infection.

Cardiovascular implants are exposed to a range of shear stress generated by blood flow. Adhesion of cells and bacteria on the biomaterial surface is in part mediated by these shear forces which may contribute to the persistence of device-centered infection. Previous studies have shown that *S. epidermidis* is capable of adhesion on polyetherurethane ureas under shear stress levels as high as 70 dynes/cm^2 and is independent of shear stress.[7] In contrast, leukocyte adhesion on polyetherurethane ureas is sensitive to shear stress and minimal at levels of shear stress >7 dynes/cm^2.[8–10] As a result, leukocytes would be unable to interact with bacteria because of the lack of leukocyte

Correspondence to: Y. Iwasaki; e-mail: yasu.org@tmd.ac.jp
Contract grant sponsor: National Institutes of Health; contract grant number: EB-00279

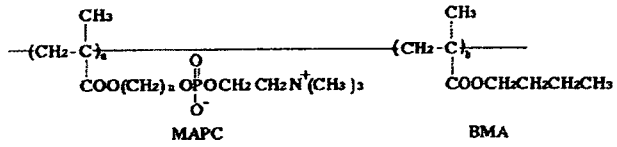

Figure 1. Chemical structure of phospholipids polymers coated onto PET sheets.

adhesion at shear stresses >7 dynes/cm^2 permitting bacteria to colonize on biomaterials.

To facilitate the success of a biomaterial, polymer surfaces can be modified with poly[ω-methacryloyloxyalkyl phosphorylcholine (MAPC)-*co*-*n*-butyl methacrylate (BMA)] to influence material properties and potentially reduce adherent bacteria. At the same time, these surface properties can direct leukocyte adhesion onto the surface, which may also contribute to persistence of biomaterial infection. Poly[2-methacryloyloxyethyl phosphorylcholine (MPC)-*co*-BMA] (PMB) was created to mimic biological membranes that do not cause cell and blood protein adsorption or activation upon contact.[11,12] The MAPC copolymers have been shown to reduce platelet adhesion and activation[13–15] as well as suppress an inflammatory response of adherent cells.[16,17] The excellent compatibility of these materials has been correlated to a strong affinity for phospholipids from human plasma and low protein adsorption.[18–24]

In this study, the effects of the phospholipid polymer surfaces on the adhesion of bacteria and leukocytes under dynamic flow conditions were examined to further elucidate the mechanisms of persistent biomaterial infection. MAPC copolymers were synthesized to contain varying methylene chain lengths, which is the spacer connecting the phosphorylcholine group. Therefore, the effect of the chemical structure of the phosphorylcholine moiety on bacterial and leukocyte adhesion was evaluated.[13]

MATERIALS AND METHODS

Phospholipid polymers surfaces

Polyethylene terephthalate (PET) surfaces were coated with a phospholipid polymer, MAPC-*co*-BMA, in a 0.3 mole fraction of the MAPC unit (Fig. 1). Copolymerization of MAPC and BMA was performed in an ethanol solution with α,α'-azobisisobutyronitrile (AIBN) as an initiator. The phospholipid polymer materials used in this study contained varying methylene chain lengths between the phospholipid polar head and the backbone in the MAPC segment. The material designated poly($MPC_{0.3}$-*co*-$BMA_{0.7}$) (PMB30) contains a methylene chain length, $(CH_2)n$, of n = 2, whereas poly[6-methacryloyloxyhexyl phosphorylcholine $(MHPC)_{0.3}$-*co*-$BMA_{0.7}$] (PMHB30) contains a chain length of n = 6 (Table I). The PET-based materials were cut into 17-mm discs, cleaned with distilled water, sterilized with ethylene oxide gas, and equilibrated in phosphate-buffered saline (PBS) overnight.

Rotating disk system (RDS)

The RDS (Pine Instrument Company) provides a useful *in vitro* model to study cell–biomaterial interactions under well-defined flow fields, which has been detailed in previous studies.[8,25] Based on the radial distance from the center of the disk surface, the system generates a range of shear stress across the surface of the material. Fluid approaches the surface of the disk with constant mass flux which transports the cells or bacteria uniformly to the rotating surface, independent of the radial position. Nearing the surface, the velocity of the fluid is increased proportional to the angular velocity of the disk. Consequently, shear stress is zero at the center of the disk and reaches a maximum at the edges.[26,27]

Components of the RDS were sterilized before conducting any experiments. Previously cut phospholipid polymer surfaces were mounted to stainless steel discs and immersed into the test media maintained at 37°C. The material was rotated at 350 rpm to generate shear stress levels of 0–18 dynes/cm^2, which are within the physiological range in human blood vessels.[28] The experiments were conducted with a 1-h rotation period for evaluation of bacterial and neutrophil adhesion and 4 h for monocyte adhesion.

Bacterial adhesion

A clinical isolate of a *S. epidermidis* bacterial strain RP62A (ATCC 35984) was cultured in tryptic soy broth (Becton Dickinson) overnight at 37°C in an orbital shaker. Subsequent to washing and resuspension in PBS, the bacterial concentration was quantified in colony-forming units per milliliter (cfu/mL) using an optical density measurement at 550 nm by an automated microplate reader (Biotek Instruments). The bacteria was injected at a concentration of 10^8 cfu/mL into a test suspension of either PBS or 25% pooled human serum in the RDS at the start of rotation. Upon rotation for a 60-min time period, a fluid transfer method was used to remove excess nonadherent bacteria from the test suspension. The adherent bacteria were fixed on the polymer surface with 2.5% glutaraldehyde overnight and prepared with serial ethanol drying for scanning electron microscopy (SEM) analysis. The samples were sputter coated and analyzed with SEM for bacterial density measurements at individual shear stress levels.

TABLE I
Phospholipid Polymer Surfaces

Material	Base	Copolymer	Methylene Chain Length
PET	—	—	—
PMB30	PET	Poly(MAPC-*co*-BMA)	2
PMHB30	PET	Poly(MAPC-*co*-BMA)	6

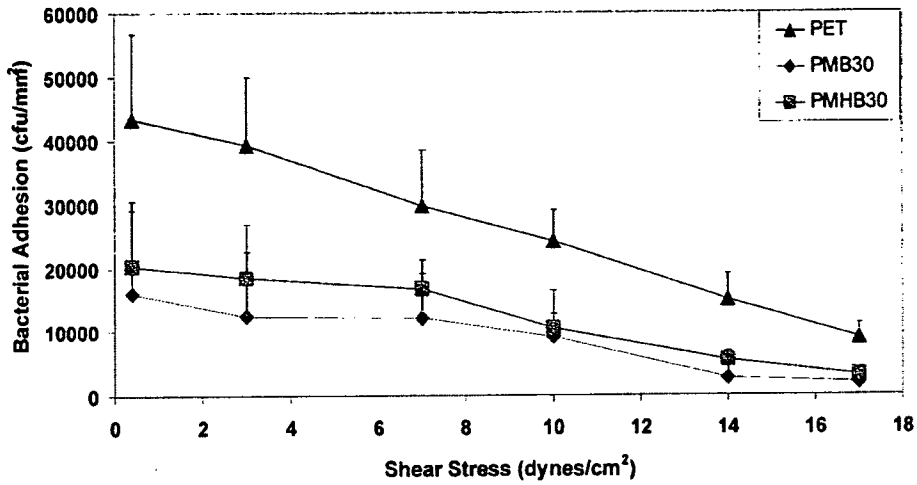

Figure 2. Bacterial adhesion in PBS under shear stress. Data represent the mean + SD; $n = 3$.

Neutrophil adhesion

Neutrophils were isolated from whole human blood drawn from unmedicated donors using sodium citrate (Sigma Chemical Co.) as an anticoagulant following a previously published technique.[29] Briefly, Ficoll-Paque (Pharmacia Biotech) was used for density gradient centrifugation of the citrated blood, followed by incubation on ice in Dextran T700 (Pharmacia Biotech) for sedimentation, and finally hypotonic lysis of remaining red blood cells. The isolated neutrophils were washed and resuspended in RPMI Medium 1640 (GIBCO). Viability and concentration of freshly isolated neutrophils were determined using the trypan blue exclusion assay. Neutrophil viability was found to be >98%. A concentration of 2×10^6 cells/mL neutrophils was pipetted into a test suspension of either RPMI Medium 1640 or 25% autologous human serum in RPMI Medium 1640 in the RDS. Because of the presence of anticoagulants in human plasma, which can reduce integrin-mediated cell adhesion, autologous serum was chosen for use in our study instead of human plasma. Upon rotation for a 60-min time period, a fluid transfer method was used to remove excess nonadherent cells from the test suspension. The adherent neutrophils were fixed with 2.5% glutaraldehyde overnight and prepared with serial ethanol drying. Each surface was analyzed with SEM and the cell density calculated for individual shear levels.

Monocyte adhesion

Blood was drawn from unmedicated donors using 0.4% sodium citrate for anticoagulation. Human peripheral blood monocytes were isolated according to a published technique using density gradient centrifugation.[30] The isolated monocytes were washed and resuspended in RPMI Medium 1640 and monocyte viability and concentration were assessed using trypan blue exclusion. A concentration of 1×10^6 cells/mL monocytes was pipetted into a test suspension of the RDS which contained either RPMI Medium 1640 or 25% human serum in RPMI Medium 1640. After a 4-h rotation period, excess nonadherent cells were removed from the test suspension by fluid transfer. The adherent monocytes were fixed and analyzed with SEM for cell density measurements at individual shear levels.

Statistical analysis

The data are represented as the mean + the standard deviation (SD). Statistical comparisons were conducted by performing analysis of variance on the data using Statview 5.0.1 (SAS Institute).

RESULTS

Bacterial adhesion

Bacterial adhesion was examined on the phospholipid polymer surfaces in PBS and 20% human serum under shear stress conditions. *S. epidermidis* adhesion in PBS was found to be shear stress dependent with decreasing adhesion at higher shear stresses (Fig. 2). Material surface chemistry also influenced bacterial adhesion, more specifically, the presence of the phospholipid polymers reduced bacterial adhesion in PBS. Furthermore, bacterial adhesion was significantly lower on PMB30 ($p = 0.0008$), and the other phospholipid polymer surface, PMHB30 ($p = 0.0021$) in comparison to the control, PET (Fig. 2). Therefore, the length of the methylene chain on the MAPC unit influenced bacterial adhesion with the shorter chain length restricting bacterial adhesion most effectively. The reduction in adhesion can be observed in the SEM micrographs in Figure 3. However, bacterial adhesion in the presence of serum was noticeably reduced to <10%

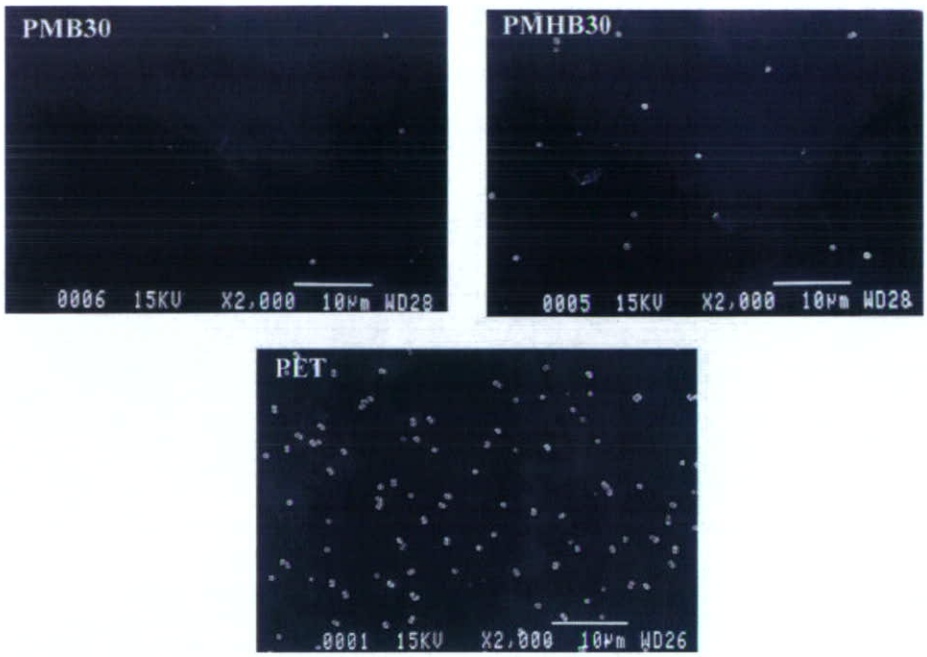

Figure 3. SEM micrographs of *S. epidermidis* adhesion in PBS in the region of lower shear stress on PET and PET surfaces modified with MAPC copolymers.

in comparison to adhesion in PBS media (Fig. 4). Additionally, the presence of serum proteins eliminated shear and surface dependent bacterial adhesion.

Leukocyte adhesion

Leukocyte adhesion was examined on the phospholipid polymer surfaces in cell media and 25% human serum. The results showed that, in cell culture medium deficient of serum proteins, monocyte and neutrophil adhesion was minimal to none (data not shown). In contrast, trends for neutrophil adhesion in the presence of serum proteins demonstrated shear dependence with decreasing adhesion up to 10 dynes/cm^2 (Fig. 5). The neutrophil adhesion profile for PMB30 shows minimal shear stress dependence with adhesion remaining close to zero after 7 dynes/cm^2.

Similar to bacterial adhesion in PBS, PMB30 significantly reduced neutrophil adhesion in comparison to the control PET (p = 0.0163). SEM micrographs in Figure 6 demonstrate low neutrophil adhesion on the phospholipid polymer surfaces.

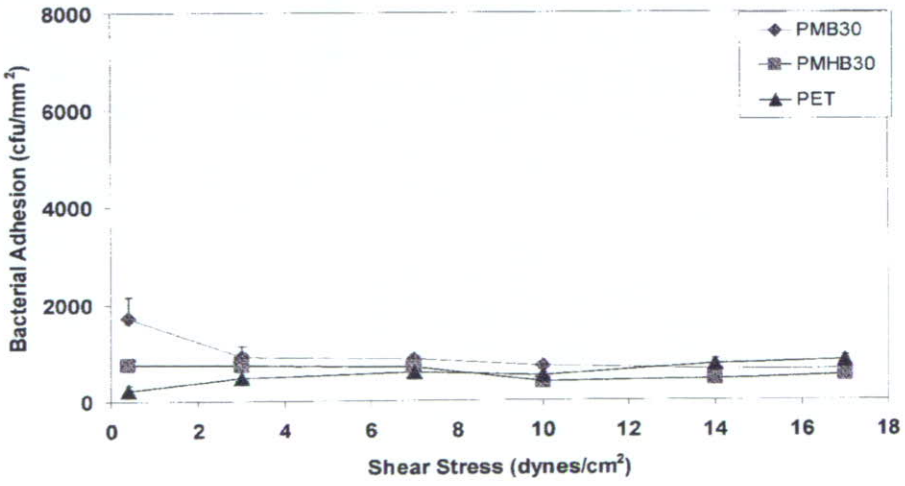

Figure 4. Bacterial adhesion in the presence of serum under shear stress. Data represent the mean + SD; n = 3.

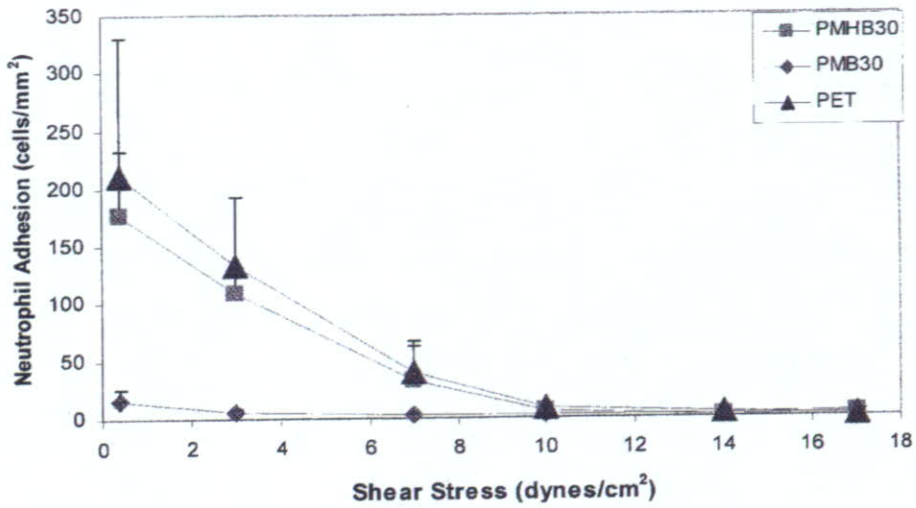

Figure 5. Neutrophil adhesion in the presence of serum under shear stress. Data represent mean + SD; $n = 3$.

Monocyte adhesion in the presence of serum also exhibited shear stress dependence which decreased sharply up to 7 dynes/cm^2 (Fig. 7). Modification of the PET surfaces with MAPC copolymers reduced monocyte adhesion with the lowest cell density exhibited on PMB30 (Fig. 8). Adhesion remained minimal on PMB30 throughout the range of shear stresses with less shear stress dependence observed in comparison to the other materials. In general, leukocytes adhered in a differential, shear-dependent manner as a result of distinct material surface chemistries with minimal adhesion occurring on PMB30, the surface composed of MAPC copolymers with the shorter methylene chain length.

DISCUSSION

Device-associated infection is initiated by firm bacterial adhesion to the implant surface, followed by colonization and biofilm formation. The presence of the implant and bacterial invasion stimulate the host response causing leukocytes to migrate to the vicinity

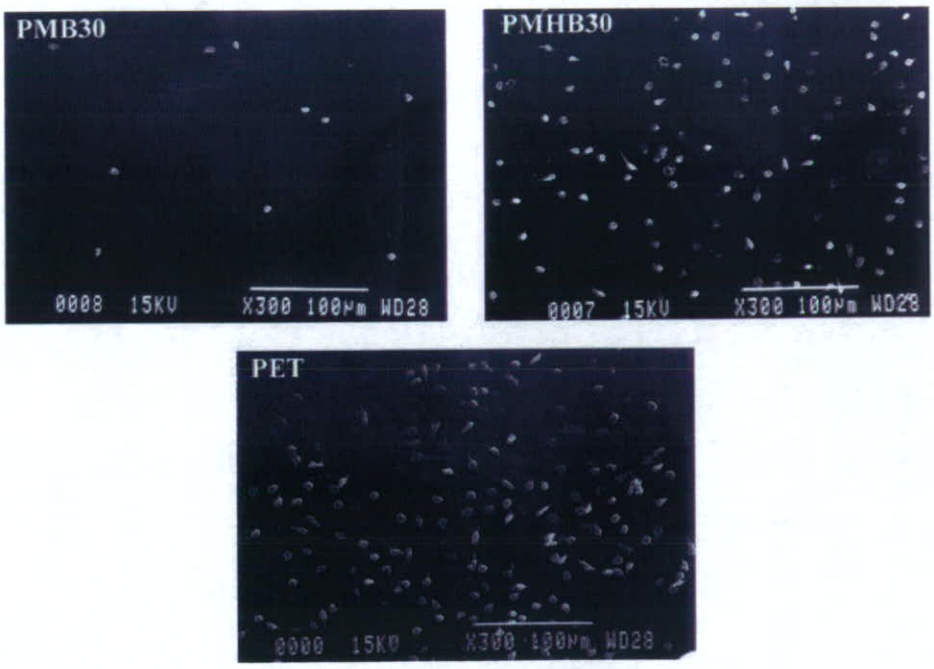

Figure 6. SEM micrographs of neutrophil adhesion in serum on PET and PET surfaces modified with MAPC copolymers.

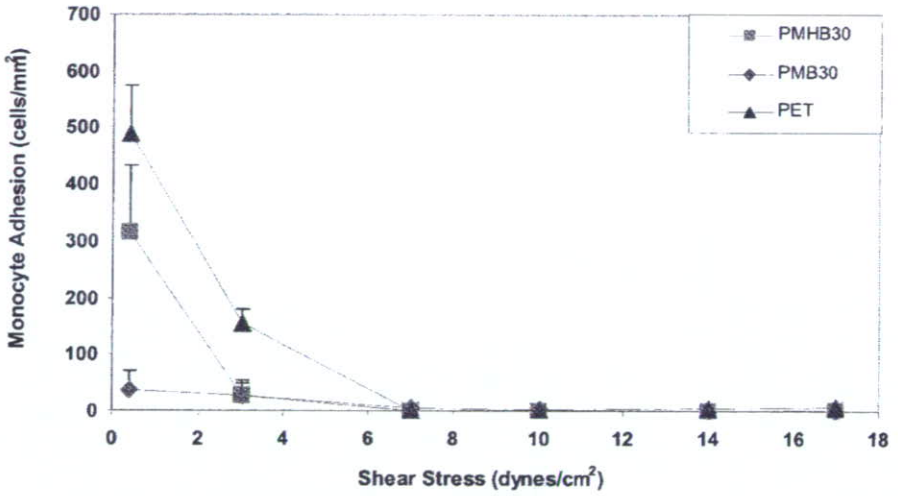

Figure 7. Monocyte adhesion in the presence of serum under shear stress. Data represent mean + SD; $n = 3$.

of the implant.[1–4] At the material interface, surface properties of the biomaterial and the local hydrodynamic environment can govern bacteria and cell adhesion. Surface chemistry can modulate the ability of cells to adhere to the material and fluid shear stress can influence the kinetics of adhesion, transport of cells to the surface, and rates of attachment/detachment.

Initial adhesion of *S. epidermidis* to an implant surface is dictated by reversible, nonspecific physicochemical forces and irreversible, specific ligand/receptor interactions.[7] Nonspecific interactions between bacteria and either the implant surface or proteins adsorbed on the surface are modulated by noncovalent physical forces such as short-range hydrophobic interactions which can lead to bacterial attachment.[28,31] At these proximal distances to the surface, intermolecular forces, influenced by surface properties of the material, including surface energy, chemical composition, local media components, and hydrodynamic conditions, can increase or reduce the adhesive capacity of the bacteria. Adhesion in PBS is restricted to nonspecific interactions between the bacteria and the surface. In this study, results showed that bacterial adhesion was mediated by shear stress. Furthermore, modification of the PET surface with the MAPC co-

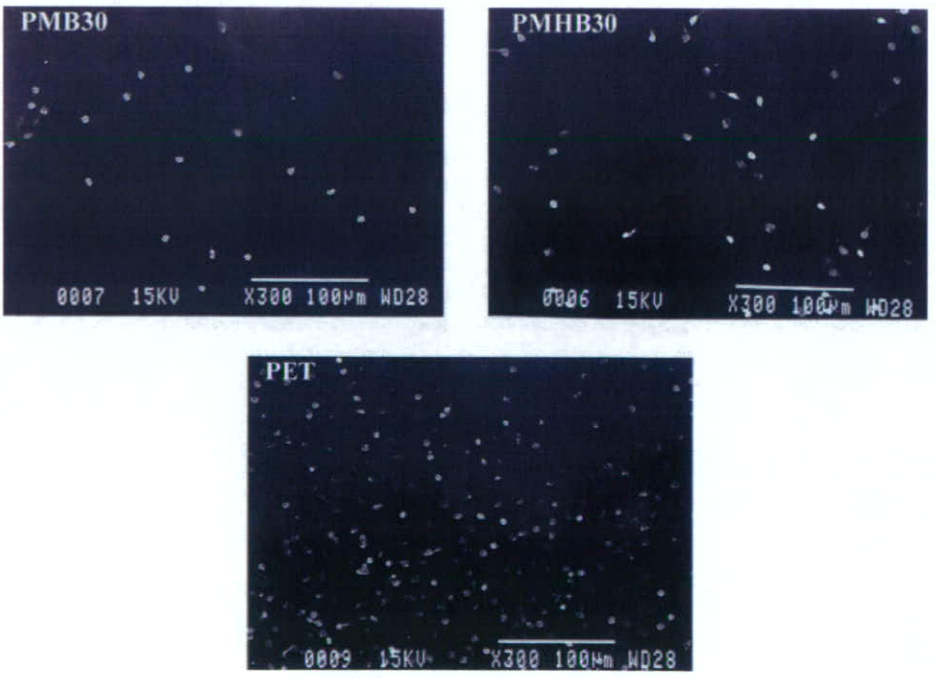

Figure 8. SEM micrographs of monocyte adhesion in serum on PET and PET surfaces modified with MAPC copolymers.

polymers resulted in reduced bacterial adhesion compared with the control PET. At low shear stress levels, nonspecific interactions, in particular the hydrophobic attraction of the bacteria to PET, may have diminished because of the hydrophilicity of the phospholipid polar group. At high shear stresses, however, the physical forces of flow dominated resulting in reduced bacterial adhesion on all materials. The chemical structure of the phosphorylcholine moiety also affected bacterial adhesion with significantly reduced adhesion observed on the MAPC copolymer materials with the shorter methylene chain length.

Specific ligand–receptor interactions were evaluated with bacterial adhesion in pooled human serum. Because of rapid kinetics, a layer of proteins adsorbs within seconds onto the surface of a biomaterial. Results from this study demonstrated that the presence of serum proteins eliminated shear stress and surface chemistry-dependent bacterial adhesion, which is in agreement with other published work.[8,32–34] Many studies have shown that protein adsorption is inhibited on the MAPC copolymer modified surfaces.[13,19,20,35–37] The reduced protein adsorption is attributed to the strong affinity of the MAPC copolymers for phospholipids in human plasma.[17,18,24,38–40] However, levels of bacterial adhesion in serum were <10% of adhesion observed in PBS and independent of shear stress and surface chemistry effects. Consequently, protein adsorption may have a greater impact on limiting or inhibiting initial bacterial adhesion, despite reduced protein adsorption on the phospholipid polymer surfaces. Therefore, the MAPC copolymers on the phospholipid surfaces possibly had negligible effects on the reduced bacterial adhesion observed in the presence of serum proteins.

Leukocyte adhesion was analyzed in the presence of serum proteins to investigate adhesion mediated by specific ligand–receptor interactions. Leukocyte adhesion was determined to be sensitive to shear stress and material surface chemistry. A decrease in monocyte and neutrophil adhesion was observed on the MAPC-modified materials, possibly because of a reduction in protein adsorption on the phospholipid polymer surfaces. Similar results were observed with reduced neutrophil adhesion on phosphorylcholine-rich surfaces.[41] The results from this study also show that leukocyte adhesion throughout the range of shear stress was lowest on PMB30, the MAPC copolymer surface with the shorter methylene chain length.

CONCLUSION

Surface modification of PET with MAPC copolymers reduced the levels of bacterial and leukocyte adhesion. Furthermore, varying the methylene chain length of the material influenced bacterial and cellular adhesion where a shorter methylene chain length resulted in decreased adhesion. The proposed mechanism for inhibition of leukocyte adhesion is attributed to an organized layer of phospholipids assembling onto the surface of the biomaterial, which serves to reduce protein adsorption and, consequently, creates a biocompatible, infection-resistant material.

References

1. Sugarman B, Young EJ. Infections associated with prosthetic devices: magnitude of the problem. Infect Dis Clin Am 1989; 3:187–198.
2. Gray ED, Peters G, Verstegen M, Regelman WE. Effect of extracellular slime substance from *Staphylococcus epidermidis* on the human cellular immune response. Lancet 1984;1:365–367.
3. Gristina AG, Hobgood CD, Webb LX, Myrvik QN. Adhesive colonization of biomaterials and antibiotic resistance. Biomaterial 1987;8:423–426.
4. Higashi JM, Marchant RE. Implant infections. In: Recum AFV, editor. Handbook of biomaterials evaluation. Washington, DC: Taylor & Francis; 1999. p 493–506.
5. von Eiff C, Peters G, Heilmann C. Pathogenesis of infections due to coagulase-negative staphylococci. Lancet Infect Dis 2002;3:677–685.
6. Costerton JW, Lewandowski Z, Caldwell DE, Korber DR, Lappin-Scott HM. Microbial biofilms. Annu Rev Microbiol 1995; 49:711–745.
7. Wang IW, Anderson JM, Marchant RE. *Staphylococcus epidermidis* adhesion to hydrophobic biomedical polymer is mediated by platelets. J Infect Dis 1993;167:329–336.
8. Shive MS, Hasan SM, Anderson JM. Shear stress effects on bacterial adhesion, leukocyte adhesion, and leukocyte oxidative capacity on a polyetherurethane. J Biomed Mater Res 1999;46:511–519.
9. Shive MS, Brodbeck WG, Colton E, Anderson JM. Shear stress and material surface effects on adherent human monocyte apoptosis. J Biomed Mater Res 2002;60:148–158.
10. Sapatnekar S, Kao WJ, Anderson JM. Leukocyte-biomaterial interactions in the presence of *Staphylococcus epidermidis*: flow cytometric evaluation of leukocyte activation. J Biomed Mater Res 1997;35(4):409–420.
11. Ishihara K, Ueda T, Nakabayashi N. Preparation of phospholipids polymers and their properties as hydrogel sheet. Polym J 1990;22:355–360.
12. Gong Y, Luo L, Petit A, Zukor DJ, Huk OL, Antoniou J, Winnick FM, Mwale F. Adhesion of human U937 macrophages to phosphorylcholine-coated surfaces. J Biomed Mater Res 2005;72A:1–9.
13. Iwasaki Y, Kurita K, Ishihara K, Nakabayashi N. Effect of methylene chain length in phospholipid moiety on blood compatibility of phospholipid polymers. J Biomater Sci Polym Ed 1994;6(5):447–461.
14. Iwasaki Y, Mikami A, Kurita K, Yui N, Ishihara K, Nakabayashi N. Reduction of surface-induced platelet activation on phospholipid polymer. J Biomed Mater Res 1997;36:508–515.
15. Iwasaki Y, Nakabayashi N, Ishihara K. Preservation of platelet function on 2-methacryloyloxyethyl phosphorylcholine-graft polymer as compared to various water-soluble graft polymers. J Biomed Mater Res 2001;57:72–78.
16. Sawada S, Sakaki S, Iwasaki Y, Nakabayashi N, Ishihara K. Suppression of the inflammatory response from adherent cells

on phospholipid polymers. J Biomed Mater Res 2003;64A:411–416.
17. Moro T, Takatori Y, Ishihara K, Konno T, Takigawa Y, Matsushita T, Chung UI, Nakamura K, Kawaguchi H. Surface grafting of artificial joints with a biocompatible polymer for preventing periprosthetic osteolysis. Nat Mater 2004;3:829–836.
18. Ueda T, Watanabe A, Ishihara K, Nakabayashi N. Protein adsorption on biomedical polymers with a phosphorylcholine moiety adsorbed with phospholipid. J Biomater Sci Polym Ed 1991;3:185–194.
19. Tanaka S, Iwasaki Y, Ishihara K, Nakabayashi N. Assessment of adsorption of liposomes on a phospholipid polymer surface using a quartz crystal microbalance. Macromol Rapid Commun 1994;15:319–326.
20. Ishihara K, Ziats NP, Tierney BP, Nakabayashi N, Anderson JM. Protein adsorption from human plasma is reduced on phospholipid polymers. J Biomed Mater Res 1991;25:1397–1407.
21. Ishihara K, Oshida H, Endo Y, Ueda T, Watanabe A, Nakabayashi N. Hemocompatibility of human whole blood on polymers with a phospholipid polar group and its mechanism. J Biomed Mater Res 1992;26:1543–1552.
22. Iwasaki Y, Tanaka S, Hara M, Ishihara K, Nakabayashi N. Stabilization of liposomes attached to polymer surfaces having phosphorylcholine groups. J Colloid Interface Sci 1997;192:432–439.
23. Iwasaki Y, Nakabayashi N, Nakatani M, Mihara T, Kurita K, Ishihara K. Competitive adsorption between phospholipid and plasma protein on a phospholipid polymer surface. J Biomater Sci Polym Ed 1999;10(5):513–529.
24. Stossel TP, Pollard TD, Mason RJ, Vaughan M. Isolation and properties of phagocytic vesicles from polymorphonuclear leukocytes. J Clin Invest 1971;50:1745–1747.
25. Kleinstreuer C. Engineering fluid dynamics. New York: Cambridge University Press; 1997.
26. Levich VG. Physicochemical hydrodynamics. Englewood Cliffs, NJ: Prentice Hall; 1962.
27. Wootton DM, Ku DN. Fluid mechanics of vascular systems, diseases, and thrombosis. Annu Rev Biomed Eng 1999;1:299–329.
28. Bos R, van der Mei HC, Busscher HJ. Physico-chemistry of initial microbial adhesive interactions: its mechanisms and methods for study. FEMS Microbiol Rev 1999;23:179.
29. Shive MS, Salloum ML, Anderson JM. Shear stress-induced apoptosis of adherent neutrophils: a mechanism for persistence of cardiovascular device infections. Proc Natl Acad Sci USA 2000;97(12):6710–6715.
30. McNally AK, Anderson JM. Complement C3 participation in monocyte adhesion to different surfaces. Proc Natl Acad Sci USA 1994;91:10119–10123.
31. Dickinson GM, Bisno AL. Infections associated with indwelling devices: concepts of pathogenesis; infections associated with intravascular devices. Antimicrob Agents Chemother 1989;33(5):597–601.
32. Sapatnekar S, Kieswetter KM, Merritt K, Anderson JM, Cahalan L, Verhoeven M, Hendriks M, Fouache B, Cahalan P. Blood-biomaterial interactions in a flow system in the presence of bacteria: effect of protein adsorption. J Biomed Mater Res 1995;29:247–256.
33. Dickinson RB, Nagel JA, Proctor RA, Cooper SL. Quantitative comparison of shear-dependent *Staphylococcus aureus* adhesion to three polyurethane ionomer analogs with distinct surface properties. J Biomed Mater Res 1997;36:152–162.
34. Iwasaki Y, Sawada S, Nakabayashi N, Khang G, Lee HB, Ishihara K. The effect of the chemical structure of the phospholipid polymer on fibronectin adsorption and fibroblast adhesion on the gradient phospholipid surface. Biomaterials 1999;20:2185–2191.
35. Ishihara K, Tsuji T, Kurosaki T, Nakabayashi N. Hemocompatibility on graft copolymers composed of poly(2-methacryloyloxyethyl phosphorylcholine) side chain and poly(*n*-butyl methacrylate) backbone. J Biomed Mater Res 1994;28:225–232.
36. Ishihara K, Oshida H, Endo Y, Watanabe A, Ueda T, Nakabayashi N. Effects of phospholipid adsorption on nonthrombogenicity of polymer with phospholipid polar group. J Biomed Mater Res 1993;27:1309–1314.
37. Iwasaki Y, Kurita K, Ishihara K, Nakabayashi N. Effect of reduced protein adsorption on platelet adhesion at the phospholipid polymer surfaces. J Biomater Sci Polym Ed 1996;8:151–163.
38. Ishihara K, Nomura H, Mihara T, Kurita K, Iwasaki Y, Nakabayashi N. Why do phospholipid polymers reduce protein adsorption? J Biomed Mater Res 1998;39:323–330.
39. Tegoulia VA, Cooper SL. Leukocyte adhesion on model surfaces under flow: effects of surface chemistry, protein adsorption, and shear rate. J Biomed Mater Res 2000;50:291–301.
40. Yung LY, Cooper SL. Neutrophil adhesion on phosphorylcholine-containing polyurethanes. Biomaterials 1998;19:31–40.

Selective Cell Attachment to a Biomimetic Polymer Surface through the Recognition of Cell-Surface Tags

Yasuhiko Iwasaki,*,† Emi Tabata,†,§ Kimio Kurita,§ and Kazunari Akiyoshi†,‡

Institute of Biomaterials and Bioengineering, Tokyo Medical and Dental University, 2-3-10, Kanda-surugadai, Chiyoda-ku, Tokyo 101-0062, Japan, Center of Excellence Program for Frontier Research on Molecular Destruction and Reconstruction of Tooth and Bone, Tokyo Medical and Dental University, 2-3-10, Kanda-surugadai, Chiyoda-ku, Tokyo 101-0062, Japan, and Department of Materials and Applied Chemistry, College of Science and Technology, Nihon University, 1-8-14, Kanda-surugadai, Chiyoda-ku, Tokyo 101-8308, Japan. Received December 7, 2004; Revised Manuscript Received March 18, 2005

Reactive phosphorylcholine polymers, which can recognize biosynthetic cell-surface tags, were synthesized to control cell attachment. Human promyelocytic leukemia cells (HL-60) with unnatural carbohydrates as cell-surface tags were harvested by treatment with *N*-levulinoylmannosamine (ManLev). The attachment of ManLev-treated HL-60 cells to 2-methacryloyloxyethyl phosphorylcholine (MPC) polymers with hydrazide groups was studied. HL-60 cells, which are nonadhesive, did not attach to any polymer surface without ManLev treatment. In contrast, ManLev-treated HL-60 cells attached to a poly[MPC-*co*-*n*-butyl methacrylate (BMA)-*co*-methacryloyl hydrazide (MH)] (PMBH) surface following 15 min of incubation. The cells that attached to the PMBH surface retained their native morphology and viability for 24 h of incubation. On the other hand, approximately half of the HL-60 cells that attached to the poly(BMA-*co*-MH) (PBH) surface died. These results suggest that MH units in the polymer act as anchors for cell attachment and MPC units help to preserve cell viability on a polymer surface. The coculture of ManLev-treated HL-60 and fluorescence-stained human uterine cervical cancer cells (HeLa) was carried out on polymer surfaces. ManLev-treated HL-60 cells specifically attached to the PMBH surface. In contrast, both HL-60 and HeLa cells were observed on the PBH surface. The control of cellular interactions with synthetic polymers may be useful for the future development of cell-integrated biosensors and biomedical devices.

INTRODUCTION

Synthetic polymers capable of selectively recognizing proteins or cells play important roles in cell separation, biosensors, and the development of biomedical materials (*1*, *2*). In general, few synthetic polymers can recognize a specific biomolecule or cell in vivo because of the complexity of the environment.

Using physicochemical and biological approaches, various surface conditions, such as a wettability gradient (*3*), topological patterns (*4*, *5*), and peptide-immobilization (*6*–*13*) have been applied to control cell attachment. Particularly, Arg-Gly-Asp (RGD)-immobilized surfaces have been extensively studied to control cell adhesion with ligand–receptor interactions (*6*, *11*–*13*). While these approaches have been quite successful, the selectivity of RGD is limited because the RGD sequence is not unique for a specific cell. Moreover, the control of cell attachment to a solid surface has been mainly studied with adhesive cells, and there have been few reports on systems for nonadhesive cells such as leukemia cells (*14*).

Synthetic polymers with an affinity for a cell surface at a submolecular level may be useful for controlling cell/polymer interactions (*15*). Most of these polymers are water-soluble and are used to immobilize the cell surface. For example, lipophilic anchors (*14*), chemical immobilization (*16*, *17*), and ligand–receptor interactions (*18*) have been studied. Through fixation of these polymers on solid surfaces, controlled cell attachment can be achieved. However, the recognition of a specific cell by a synthetic polymer is still limited because most of the cell/polymer interactions proposed are seen with a wide variety of cells, in contrast to unique interaction with a specific cell type. Also, some approaches cannot be applied under physiological conditions because nonspecific interaction with plasma protein often interferes with the specificity of materials for a cell membrane.

In a living cell, carbohydrates on the cell surface contribute to most communications between the cell and its environment (*19*). Therefore, it may be possible to control cell functions with polymers, which can affect carbohydrate interaction with a cell surface. For the recognition of a specific cell, tagging of carbohydrates on the cell membrane, as well as the polymer design, may be effective.

The incorporation of unnatural carbohydrates into living cells provides an opportunity to study the specific contributions of sialic acid and its *N*-acyl side chains to sialic acid-dependent ligand–receptor interactions at a submolecular level. Bertozzi and co-workers have expressed unnatural functional groups, i.e., acetyl, levulinoyl, and azideacetyl groups, on living cell surfaces through the glycosylation of unnatural monosaccharides (*20*–*23*). Since the initial demonstration of cell-surface engineering with *N*-levulinoylmannosamine (ManLev),

* Corresponding author. Phone: +81-3-5280-8026. Fax: +81-3-5280-8027. E-mail: yasu.org@tmd.ac.jp.

† Institute of Biomaterials and Bioengineering, Tokyo Medical and Dental University.

‡ Center of Excellence Program for Frontier Research on Molecular Destruction and Reconstruction of Tooth and Bone, Tokyo Medical and Dental University.

§ Nihon University.

10.1021/bc049707r CCC: $30.25
Published on Web 04/16/2005

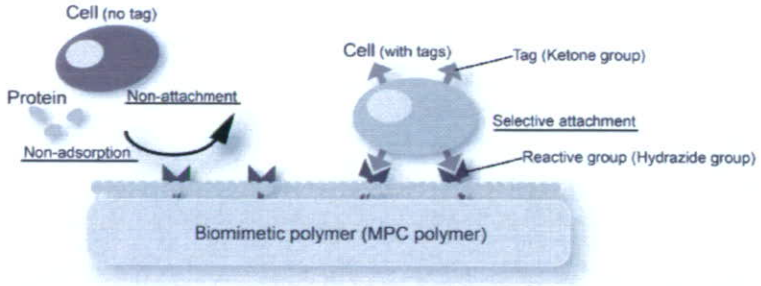

Figure 1. Schematic representation of specific cell attachment to a nonfouling MPC polymer surface through cell-surface tags.

Table 1. Results of Polymer Synthesis

abbrev	molar fraction of units (MPC/BMA/MH) in feed	molar fraction of units (MPC/BMA/MH) in copolymer	conversion,[a] %	M_w[b] ($\times 10^{-4}$)	M_w/M_n[b]	surface mole fraction of coating sample[c] (MPC/BMA/MH)
PMB	0.30/0.70/-	0.30/0.70/-	–	–	–	0.37/0.63/-
PMBH0.5	0.295/0.70/0.005	0.287/0.71/0.003	48.0	–	–	0.34/0.64/0.02
PMBH2	0.28/0.70/0.02	0.26/0.73/0.01	47.8	13.9	2.4	0.13/0.82/0.05
PMBH5	0.20/0.70/0.10	0.18/0.77/0.05	18.3	4.6	2.4	0.25/0.71/0.04
PMBH10	0.25/0.70/0.05	−0.19/0.74/0.07	80.6	8.2	2.9	0.22/0.74/0.04
PBH2	−/0.98/0.02	−/0.98/0.02	64.6	5.9	1.9	−/0.95/0.05
PBH5	−/0.95/0.05	−/0.98/0.02	58.5	5.1	1.6	−/0.94/0.06
PBMA[d]	−/1.00/−	−/1.00/−	–	33.7	–	−/1.00/−

[a] [monomer] = 1.0 M, [AIBN] = 0.5 mM, polymerization temperature 60 °C. [b] Determined by GPC. [c] Determined by XPS. [d] Purchased from Aldrich.

this technique has been applied to the development of targeted imaging reagents (*24*) and methods for gene transfer (*25*). This tagging technique has led to great progress in cell biology and biomedical science (*26*). Sadamoto and co-workers immobilized the cell surface of bacteria using an unnatural cell-surface precursor (*27*). The adhesion of surface-engineered bacteria onto a concanavalin A-immobilized substrate has also been enhanced (*28*). The ability of noncanonical amino acids to introduce novel chemical functionalities into proteins and cells has been explored by Tirrell and co-workers (*29*–*31*). They recently reported an alternate strategy for the detection of noncanonical amino acids, in which azidohomoalanine is incorporated into the *Escherichia coli* outer membrane protein OmpC (*32*, *33*).

We have been studying 2-methacryloyloxyethyl phosphorylcholine (MPC) polymers synthesized as biomimetics of biomembrane structures (*34*–*37*). MPC polymers have a surface that resists nonspecific protein adsorption and cell adhesion, i.e., "biofouling" (*38*, *39*). Biofouling reduces the functionality of a material and can induce an unexpected bioreaction. Further, it has been shown that cells in contact with MPC polymers do not exhibit activation or an inflammatory response (*40*, *41*). However, an MPC polymer has not yet been used as a substrate for a biorecognition surface.

We report here a novel strategy for controlling selective cell attachment and detachment even in nonadhesive cells by using biomimetic polymer surface engineering and cell-surface engineering. To this end, we designed reactive biomimetic MPC polymer surfaces with hydrazide groups, which can react selectively with unnatural ketone-containing carbohydrate as a cell surface tag. Figure 1 shows a schematic representation of selective cell attachment through the recognition of a cell-surface tag. The MPC polymer surface prohibits nonspecific interaction with plasma protein that often interferes with the specificity of the interaction of materials with a cell membrane. Hydrazide groups on the MPC polymer surface react with ketone groups on the cell surface even in cell culture medium. The surface tags on living cells can be introduced in the presence of ManLev by surface engineering (*20*–*25*). In this study, we synthesized MPC polymers with hydrazide groups, prepared and characterized the polymer surface, and controlled cell attachment onto their surfaces.

MATERIALS AND METHODS

Polymer Synthesis. Methyl methacrylate and *n*-butyl methacrylate (BMA) were purified by conventional distillation. Other reagents and solvents were obtained commercially in extra-pure grade and used without further purification. 2-Methacryloyloxyethyl phosphorylcholine (MPC) was synthesized as previously reported (*42*). Methacryloyl hydrazide (MH) was synthesized by reacting methyl methacrylate (0.25 mol, 25 g) and hydrazine monohydrate (0.15 mol, 7.5 g) at 0 °C. Unreacted MMA was removed at 0 °C/10 mmHg, and MH was purified by recrystallization from toluene. ^{1}H NMR (500 MHz, ppm in $CDCl_3$) MH: 6.90 (s; NH, 1H), 5.70, 5.30(s; CH=, 1H), 3.90 (s; NH_2, 2H), 1.90 (s; CH_3, 3H).

N-Levulinoylmannosamine (ManLev) was synthesized as previously described (*21*).

Poly(MPC-*co*-BMA) (PMB), poly(BMA-*co*-MH) (PBH), and poly(MPC-*co*-BMA-*co*-MH) (PMBH) were synthesized by radical polymerization using 2,2′-azobisisobutyronitrile (AIBN) as an initiator (*38*, *42*). BMA was used as a comonomer because it makes it possible to process a polymer membrane. The mole fraction of monomer units in the polymer was determined by phosphorus analysis and elemental analysis. The number-averaged and weight-averaged molecular weight of polymers were determined with a Tosoh gel-permeation chromatography (GPC) system with a refractive index detector and size-exclusion columns (Polymer Laboratories Ltd.), MIXED-C with a poly(ethylene glycol) standard (PEG, Tosoh standard sample) in CH_3Cl/methanol (6/4,vol/vol). The results of polymerization are summarized in Table 1.

Preparation of Sample Plates for the Cell Culture Experiment. The poly(ethylene terephthalate) (PET) plates (14 mm in diameter; Wako Pure Chemical Industries, Ltd., Osaka, Japan) were immersed in an ethanol or chloroform solution of the polymer (0.5 wt %) and dried

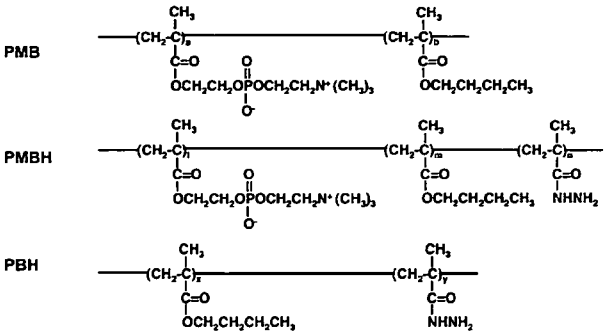

Figure 2. Chemical structures of polymers synthesized in this study.

under a vapor atmosphere of the solvent at room temperature for 30 min. This procedure was repeated twice, and the plates were then dried in vacuo. The surface properties of polymer-coated PET plates were analyzed by surface contact angle measurement (G-1; Erma, Tokyo, Japan) and X-ray photoelectron spectroscopy (XPS) (ESCA-200; Scienta, Uppsala, Sweden) with AlKα (takeoff angle 90°). Survey scan spectra of C_{1s}, O_{1s}, N_{1s}, and P_{2p} were taken.

Cell Culture Experiment. Human promyelocytic leukemia cells (HL-60) were purchased from Health Science Research Resources Bank and maintained in RPMI1640 with 10% fetal bovine serum at 37 °C in a humidified atmosphere of air containing 5% CO_2. The concentration of HL-60 was adjusted to 1.5 × 10^5 cells/mL. The medium was changed with that containing 10 mM ManLev, and the cells were stored for 3 days. The cells were then washed with fresh medium and centrifuged to remove free ManLev in the medium. The expression of ketones on the cell membrane was confirmed by fluorescence staining with 5 mM Alexa Fluor 350 hydrazide (Molecular Probes, OR).

ManLev-treated HL-60 cells were resuspended with fresh medium, and the concentration was adjusted to 1.0 × 10^5 cells/mL. The suspension (1 mL) was seeded on PMB, PMBH, and PBH and incubated for 15 min, 2, 4, and 24 h. The cells were then washed twice with fresh medium and observed by phase-contrast microscopy.

To investigate the stability of cells attached to the surface, the surface was rinsed twice with culture medium after a 2-h incubation of ManLev-treated cells on a polymer surface, and cell culture was continued for various periods.

The density of cells attached to the surface was counted in five randomly chosen areas on each polymer surface. A statistical analysis was performed with Student's *t*-test.

Sialidase Treatment. ManLev-treated HL-60 cells were in contact with PMBH5 as mentioned above. After a 2-h incubation of ManLev-treated HL-60 cells on a polymer surface, the surface was rinsed twice with fresh medium to remove nonattached cells. The polymer sample was soaked in 900 μL of fresh medium. Sialidase buffer (20mM HEPES, 140 mM NaCl, pH 6.8) was prepared, and the concentration of sialidase was adjusted to 1 U/mL. The sialidase buffer (100 μL) was added to each medium and stored at 37 °C for 30 min. The surface of the polymer was observed by phase-contrast microscopy. To identify the density of ketones on the cell membrane, cells were stained with 5 mM Alexa Fluor 488 hydrazide (Molecular Probes, Eugene, OR) and analyzed by flow cytometry (Becton Dickinson FACSCalibur).

Cytotoxicity Test. The viability of adherent HL-60 cells on a polymer surface was investigated with a LIVE/DEADViability/Cytotoxicity kit (Molecular Probes, OR). After a 2-h incubation of ManLev-treated HL-60 cells on a polymer surface, the surface was rinsed twice with fresh medium to remove nonattached cells. The cell culture was then continued for various durations. The cells attached to the polymer surface were then stained with 1 μM calcein dye and 2 μM ethidium homodimer-1 (EthD-1) dye. The samples were incubated for 15 min at 37 °C and observed by phase-contrast and fluorescence microscopy (IX-70, OLYMPUS, Tokyo, Japan). The number of attached cells and the percentage of live cells were determined in five randomly chosen areas on each polymer surface. A statistical analysis was performed with Student's *t*-test.

Coculture Experiment. Human uterine cervical cancer cells (HeLa) were purchased from Riken Cell Bank and maintained in RPMI1640 with 10% fetal bovine serum at 37 °C in a humidified atmosphere of air containing 5% CO_2. The contents of the flasks for cell maintenance were detached by trypsin treatment and a cell suspension containing 1.0 × 10^5 cells/mL in D-PBS was prepared. 5-(and-6)-Carboxyfluorescein diacetate, succinimidyl ester (CFSE, 50 μM) was added to the suspension, and the cells were stored for 15 min. The suspension was then centrifuged to remove free CFSE. CFSE-stained HeLa cells and ManLev-treated HL-60 cells were mixed in fresh medium, and their concentrations were adjusted to 1.0 X 10^4 and 1.0 × 10^5 cells/mL, respectively. The mixed cells were seeded on polymer surfaces and cocultured for 24 h. After being rinsed with the culture medium, the polymer surfaces were immediately observed by phase-contrast and fluorescence microscopy.

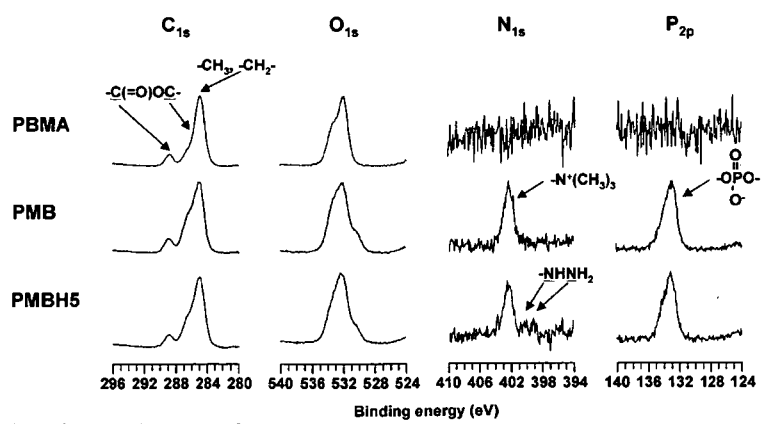

Figure 3. XPS spectra of synthetic polymer surfaces.

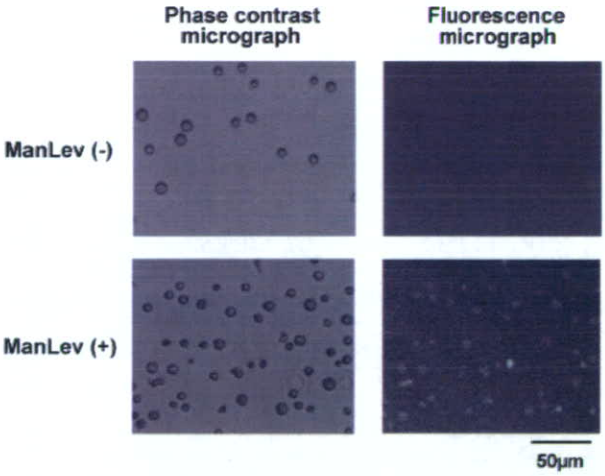

Figure 4. Fluorescence micrographs of ManLev-treated HL-60 cells stained with Alexa Fluor 350 hydrazide.

Table 2. Contact Angle Data for Polymer Surfaces

	θ_A (deg)	θ_A (deg)
PMB	92	8
PMBH0.5	87	22
PMBH2	83	16
PMBH5	93	26
PMBH10	85	25
PBH2	92	78
PBH5	92	85
PBMA	92	77

Detection of Fibronectin Adsorbed onto the Surface. The adsorption of bovine serum fibronectin from the cell culture medium onto the polymer surface was detected by a method based on the antigen/antibody reaction with enzyme-labeled immunoglobulin (*37*). Briefly, polymer-coated PET plates were placed in a 24-well tissue culture plate and secured with a silicone rubber ring. They were left in contact with PBS overnight at room temperature for equilibration of the surface. The cell culture medium was added to each well after the removal of PBS and kept there for 1 h at 37 °C; the PET plates were then rinsed with PBS. A bovine serum albumin (BSA, Sigma Chemical, St. Louis, MO) solution (1 wt % BSA in PBS) was used as a blocking reagent to inhibit any undesirable reactions and nonspecific adsorption with the following antibodies. The PET plates were kept at 4 °C for 3 h and then rinsed with PBS. After the BSA solution was removed, the plates were incubated with the primary antibodies [1 wt % BSA solution containing rabbit immunoglobulin of anti-bovine fibronectin (polyclonal, TELIOS, Pharmaceutical Inc., San Diego, CA)] for 60 min at 37 °C. The plate was rinsed with PBS. The secondary antibody (goat anti-rabbit immunoglobulin, Sigma Chemicals, St. Louis, MO) labeled with horseradish peroxidase (HRP) was then poured into each well, and the wells were stored for 60 min at 37 °C. The plates were transferred to new wells and placed in contact with 3,3′,5,5′-tetramethylbentizine (TMBZ) solution (Color formation kit, SUMILON, Tokyo, Japan) at 25 °C for 10 min in the dark. Absorbance of the TMBZ solution at 450 nm was measured using a microplate reader (Model 450, BIO-RAD Laboratories, Richmond, CA). A statistical analysis was performed with Student's *t*-test.

RESULTS AND DISCUSSION

Characterization of Polymers and Polymer Surfaces. To control cell-attachment, polymer surfaces with reactive units in a phosphorylcholine surface were designed. The hydrazide group was selected as a reaction site for a ketone group on the cell surface. Figure 2 shows the structures of polymers synthesized in this study. The polymerization of 2-methacryloyloxyethyl phosphorylcholine (MPC), *n*-butyl methacrylate (BMA), and methacryloyl hydrazide (MH) occurred in ethanol or ethanol/tetrahydrofuran (THF) mixture. As indicated in Table 1, the composition of each monomer unit could be controlled with the feed. Amphiphilic copolymers containing various amounts of hydrazide groups were obtained. PET plates coated with the synthesized polymers were prepared by the solvent evaporation technique. Elemental analysis of polymer-coated PET surfaces was performed by X-ray photoelectron spectroscopy (XPS). In the case of PET plates coated with MPC polymers, nitrogen and phosphorus peaks were observed at 402.5 and 133.0 eV, respectively (Figure 3). These are attributed to the phosphorylcholine group in the MPC units. Moreover, nitrogen peaks at 399.0 and 400.0 eV due to hydrazide groups were also observed on the surface of PMHB. The

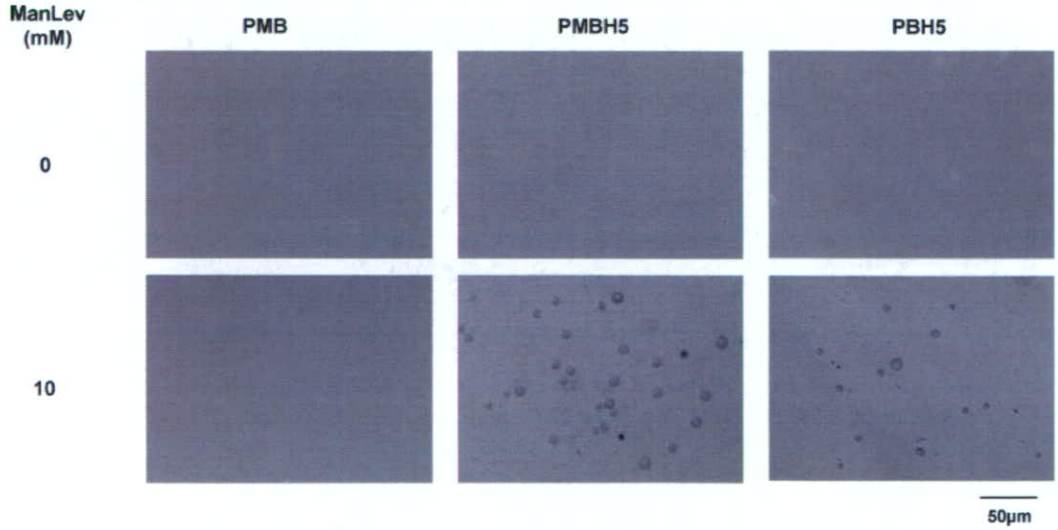

Figure 5. Phase-contrast microscopy images of polymer surfaces after contact with native and ManLev-treated HL-60 cells for 2 h.